Solid State Ionics 180 (2009) 1040–1044

Contents lists available at ScienceDirect

Solid State Ionics

journal homepage: www.elsevier.com/locate/ssi

Oxygen diffusion in $SrZrO_3$

Christelle Nivot [a], Corinne Legros [a,*], Bernard Lesage [a], Martin Kilo [b], Christos Argirusis [b,c]

[a] Univ. Paris Sud 11, Laboratoire d'Etudes des Matériaux Hors Equilibre (LEMHE-ICMMO), CNRS-UMR 8182, Bât. 410, F-91405 ORSAY Cedex, France
[b] TU Clausthal, Institut für Metallurgie, Robert-Koch-Str. 42, D-38678 Clausthal-Zellerfeld, Germany
[c] National Technical University of Athens, School of Chemical Engineering, Iroon Polytechneiou 9, Zografou, Athens, Greece

ARTICLE INFO

Article history:
Received 4 April 2007
Received in revised form 7 April 2009
Accepted 11 May 2009

Keywords:
Diffusion
^{16}O–^{18}O exchange
SIMS measurements
$SrZrO_3$

ABSTRACT

Oxygen diffusion coefficients in $SrZrO_3$ polycrystals were determined using the isotopic exchange method with ^{18}O as oxygen tracer. Diffusion treatments were performed at different temperatures between 1173 K and 1473 K. Oxygen diffusion profiles were established by secondary ion mass spectroscopy (SIMS). Classical diffusion equations were used to fit experimental results and to determine bulk diffusion (D_{vol}) and surface exchange (k) coefficients of oxygen in $SrZrO_3$ polycrystalline materials. From these values, bulk diffusion and grain boundary diffusion coefficients as well as oxygen surface exchange coefficients were determined. The activation energy of oxygen diffusion in the bulk is 2.1 eV, while for the diffusion in the grain boundary, 1.8 eV was found. The surface exchange reaction has an activation enthalpy of 1.2 eV.

1. Introduction

Perovskite type oxides ABO_3 are extensively studied and exhibit a variety of unique physical properties making them very attractive materials for many applications. Zirconates show high melting point, low thermal conductivity, high thermal expansion coefficient, thermal and chemical stability. Due to these properties, $SrZrO_3$ materials are used as thermal barrier coatings [1]. Acceptor doped $SrZrO_3$ is also known for its proton conductivity at high temperature [2,3]. This property makes $SrZrO_3$-based perovskite oxides potential materials for electrolytes in solid fuel cells and hydrogen sensors [4–7]. Another interest in $SrZrO_3$ consists in application as gate material. Indeed, thanks to high dielectric constant, low interface density and good thermal stability, $SrZrO_3$ thin films are studied in order to replace SiO_2 conventionally used in microelectronics [8] or to form MIM structure on electrodes [9]. $SrZrO_3$ is also a potential material for nuclear applications, such as inert matrix for the destruction of excess plutonium or good host material for nuclear waste storage [10]. Whatever the application concerned, interfaces exist: between electrolyte and anode/cathode in solid fuel cells, between substrate and layers in microelectronic. $SrZrO_3$ is also a (unwanted) reaction product between the cathode of a SOFC based on $(La_xSr_{1-x})Mn_yO_{3-\delta}$ (LSM) with the electrolyte, provided the composition of the LSM is improper [11]. For this reason, it is important to characterize anion diffusion at this interface by studying oxygen diffusion in polycrystalline $SrZrO_3$. However, until now, no information on oxygen diffusion in nominally undoped $SrZrO_3$ is known. Labrincha et al. [12] investigated the oxygen- and electronic conductivity on undoped, A- and B-site doped $SrZrO_3$ at temperatures between 673 K and 1173 K. The undoped material showed the lowest conductivity, both electronically as well as ionically. However, the activation enthalpy of ionic conductivity in undoped $SrZrO_3$ was very low (0.47 eV, in contrast to 1.6 eV for electronic and 1.4 eV for total conductivity), and was questioned by the authors themselves. In another work, Belyakov et al. [13] report conductivities of undoped $SrZrO_3$ obtained between 1273 K and 1773 K. The authors found an activation enthalpy of 1.1 eV for total conductivity. They investigated the influence of doping on the material and observed that on doping with cations of higher charge (W, Nb…), the conductivity can be reduced. By investigating the conductivity and TGA of 5 mol% yttrium-doped $SrZrO_3$ single crystals, Müller et al. [14] came to the conclusion that the activation enthalpy of migration of oxygen vacancies is 1.0 eV. However, their material contained significant amount of protons. Other authors reported even very high values: De Pretis et al. [15] give a value of 2.6 eV for total conductivity at 1073–1473 K. In a recent critical review, Slonimskaya and Belyakov report 2.2 eV [16]. Haile et al. [17] pointed to the necessity to know the nonstoichiometry of a perovskite conductor very well, since small deviations may affect the properties of the materials dramatically.

However, determination of oxygen transport in doped or undoped $SrZrO_3$ using tracer diffusion experiments is not done until now. De Souza et al. investigated doped $SrCeO_3$, $CaZrO_3$, and $BaCeO_3$ [18,19]. For $CaZrO_3$, activation enthalpies of 2.3 eV for diffusion and 1.9 eV for surface exchange are reported, while in $SrCeO_3$, 1.9 and 1.4 eV were found and for $BaCeO_3$ 0.9 and 0.6 eV, respectively. The activation enthalpy of surface exchange reaction is 0.7–0.8 of the activation enthalpy of (bulk) diffusion. On co-doping the cation-doped perovskites with hydrogen, the oxygen diffusion is also affected [19].

* Corresponding author. Tel.: +33 1 69 15 45 47; fax: +33 1 69 15 48 19.
E-mail address: Corinne.legros@u-psud.fr (C. Legros).

0167-2738/$ – see front matter © 2009 Elsevier B.V. All rights reserved.
doi:10.1016/j.ssi.2009.05.008

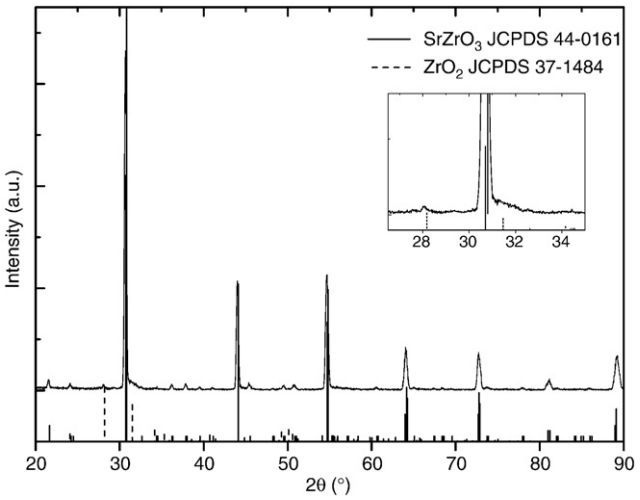

Fig. 1. X-ray diffraction pattern of $SrZrO_3$ sintered at 1773 K showing $SrZrO_3$ as the major phase and traces of monoclinic ZrO_2.

In this paper, oxygen diffusion coefficients in the bulk as well as in the grain boundary and oxygen surface exchange coefficient are determined by isotopic exchange ^{16}O–^{18}O on highly dense, nominally undoped $SrZrO_3$ ceramics. After different heating cycles between 1173 and 1473 K, depth profiles were measured by secondary ion mass spectroscopy (SIMS). These data should serve as a starting point for the investigation of doped materials, either with lower or with higher conductivity.

2. Experimental

2.1. Elaboration and characterization

$SrZrO_3$ powder was purchased from Alfa Aesar in 99.3% purity. Green pellets were produced by cold isostatic pressing (CIP) at a pressure of 250 MPa. Sintering of the samples in static air was carried out in a Lenton muffle furnace, using a linear heating ramp of 2 K min^{-1}. At the end of the ramp, the selected final temperature of 1773 K was kept for 24 h in order to obtain pellets with a density close to that of the dense material. Then samples were slowly cooled down to room temperature. Pellets were finally cut with a diamond saw from the sintered material and the surfaces were polished down to 1/4 μm with diamond pastes. An additional annealing in air was performed at 1673 K for 10 h in order to recover the damage resulting from the mechanical treatment and to reveal the microstructure (grain boundary) by thermal etching.

The crystal structure of the sintered pellets was investigated by X-ray diffraction (XRD). The XRD equipment consisted of a PANalytical X'Pert Pro MRD diffractometer with nickel-filtered Cu-$K\alpha$ radiation ($\lambda = 1.5406$ nm). Data were collected with a step size of 0.02° (2θ) and a time per step of 1.5 s. The bulk density of the sintered pellet was determined by Archimedes' method on cooled sample. A scanning electron microscope (SEM) LEICA 260 was used to characterize the microstructure of pellets. Grain size was estimated by linear intercept method on SEM micrograph.

2.2. Oxygen diffusion treatment

Oxygen diffusion was performed by means of the gas–solid isotopic exchange method, using the ^{18}O isotope as oxygen tracer. The sample was heated at 5 K min^{-1} up to selected temperature (1173 K, 1273 K, 1373 K or 1473 K) and equilibrated under ambient air during 20 h under a static atmosphere of dry air; thus, proton uptake can be excluded. Then the atmosphere was changed to 20 kPa of $^{18}O_2$ (Eurisotop, 96.7% enriched $^{18}O_2$) at the same temperature and kept static for 8 h. The first stage under air was longer than the second one under $^{18}O_2$ in order to ensure that the samples were thermodynamically equilibrated. Then the samples were cooled rapidly to room temperature under $^{18}O_2$ atmosphere.

2.3. Depth profiling by secondary ion mass spectrometry (SIMS)

The depth profiles of the secondary ion intensities [$I(^{16}O^-)$, $I(^{18}O^-)$] were collected using a CAMECA IMS 5F SIMS device (Cs^+ primary ion source with a 10 kV accelerating voltage, analysis of positive secondary ions, 5 kV secondary accelerating voltage). The diffusion profiles of the isotope ^{18}O were obtained using expression (1):

$$C(x) = \frac{I\left(^{18}O^-\right)}{I\left(^{18}O^-\right) + I\left(^{16}O^-\right)} \quad (1)$$

The depths of the craters were measured after the SIMS experiments using an Alpha Step 500 TENCOR surface profiler with a resolution of ~5 nm. Assuming uniform sputtering, the time data obtained from the SIMS were converted to distance data using the results from the crater depth measurements.

3. Results and discussion

3.1. Characterization

The XRD pattern of $SrZrO_3$ sintered at 1773 K for 24 h is shown in Fig. 1. The XRD pattern exhibits the characteristic lines of orthorhombic perovskite $SrZrO_3$ and has a high degree of crystallinity. Lattice constants of $SrZrO_3$ determined from XRD pattern are $a = 0.582$ nm, $b = 0.821$ nm, $c = 0.579$ nm, which agree very well with reported values (JCPDS 44-0161). Nevertheless, the weak line at $2\theta = 28°$ does not belong to $SrZrO_3$ but to monoclinic ZrO_2 phase (JCPDS 37-1484). It may be noted that it corresponds well to the purity of the commercial starting powder. The theoretical density derived from the lattice parameters is 5.45 g cm^{-3}. This density is slightly higher than the experimental density of 5.42 g cm^{-3}. Consequently the bulk density of the sintered body is about 99.5% of the theoretical density. The difference may be due to remaining closed pores in the sintered material as can be seen on Fig. 2 which exhibits the SEM study on the sintered sample. It is also observed from the micrograph that the material has a bimodal distribution of $SrZrO_3$ particles having primary particle sizes of ~2.5 μm and ~5.5 μm. However, such a microstructure is well suited to carry out diffusion studies [11].

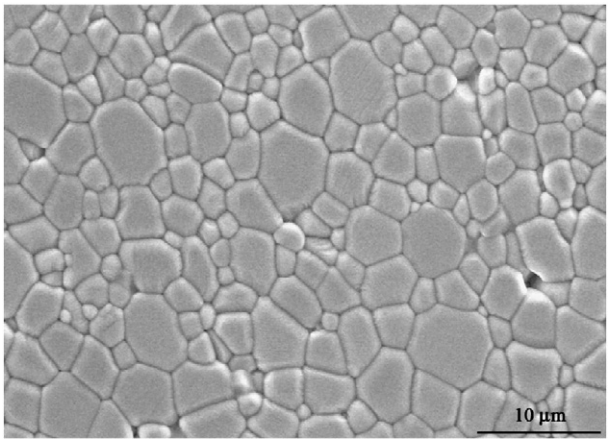

Fig. 2. SEM micrograph of $SrZrO_3$ sintered at 1773 K for 24 h.

3.2. Diffusion in polycrystalline $SrZrO_3$

3.2.1. Bulk diffusion

Under the conditions used for the isotopic exchange annealing, the oxygen isotope diffusivity D_{vol} and oxygen surface exchange rate constant k (for exchange at the interface between bulk and gas phase) were determined by fitting the obtained profiles with the appropriate solution of the diffusion equation given by Crank [21]:

$$C'(x) = \frac{C(x) - C_{bg}}{C_g - C_{bg}} = \mathrm{erfc}\frac{x}{2\sqrt{D_{vol}t}} - \exp\left(hx + h^2 D_{vol}t\right) \cdot \mathrm{erfc}\left(\frac{x}{2\sqrt{D_{vol}t}} + h\sqrt{D_{vol}t}\right) \quad (2)$$

where erfc = 1 − erf (erf the Gaussian error function), $C'(x)$ is the normalized ^{18}O concentration, $C(x)$ is the ^{18}O concentration derived from the intensity ratio of SIMS secondary ion as defined in Eq. (1), C_{bg} is the natural abundance of ^{18}O (= 0.002), C_g is the ^{18}O concentration in the gaseous phase which was fixed at $C_g = 0.967$ in all experiments, t is the annealing time, x is the depth from the surface and h is given by Eq. (3):

$$h = \frac{k}{D_{vol}} \quad (3)$$

Fig. 3 shows diffusion profiles of ^{18}O (using normalized concentration $C'(x)$ as defined in Eq. (2)) for diffusion treatments of 8 h at 1173 K, 1273 K, 1373 K and 1473 K. On this graph, scatter graphs are experimental results obtained by SIMS measurements and solid lines represent a fit according to Eq. (2). This figure proves that oxygen diffusion in $SrZrO_3$ increases with temperature. Profiles present typical profile shapes in polycrystalline materials as described e.g. by Philibert [22]: a first part which corresponds to a steep decrease of the ^{18}O concentration characteristic of bulk diffusion, and a second part with a shallow decrease of the ^{18}O concentration characteristic of grain boundaries diffusion [20]. The oxygen isotope tracer diffusivity D_{vol} and oxygen surface exchange rate constant k were determined by the fit to the part of the profile corresponding to the bulk diffusion close to surface.

Fig. 4 shows the Arrhenius plot for the oxygen bulk diffusion coefficients determined in polycrystalline $SrZrO_3$ samples. Bulk

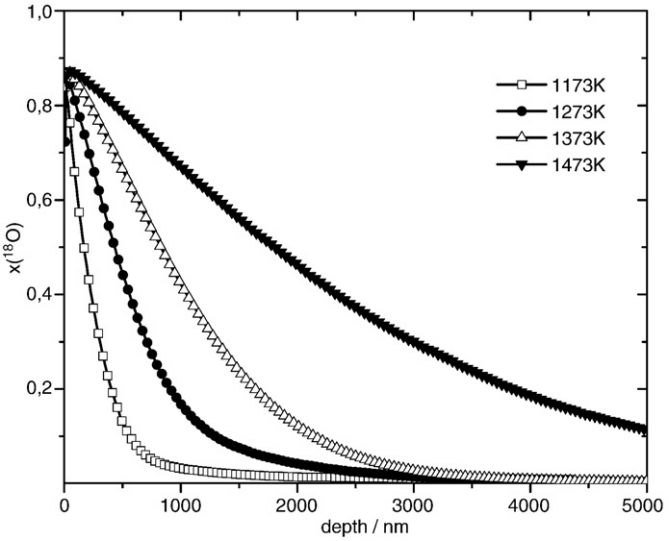

Fig. 3. Normalized concentration of ^{18}O in $SrZrO_3$ after thermal treatments at 1173 K, 1273 K, 1373 K and 1473 K.

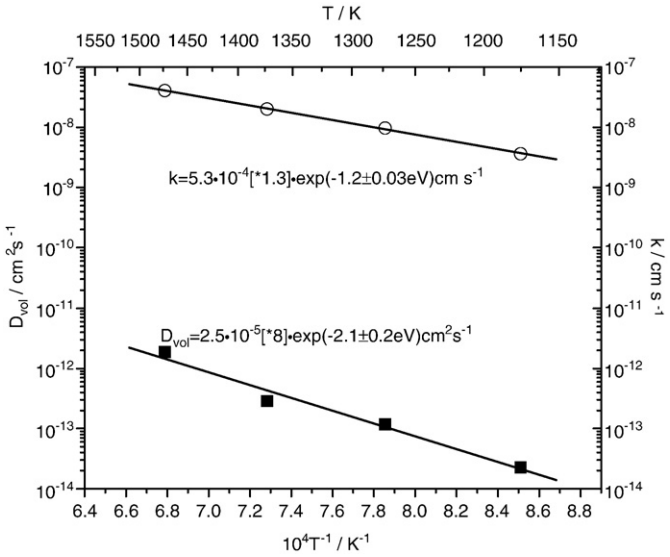

Fig. 4. Arrhenius plot of bulk diffusion coefficient D_{vol} and surface exchange coefficient k.

diffusion coefficient of oxygen and surface exchange coefficient values as plotted on Fig. 4 obey the following Arrhenius equations:

$$D_{vol} = 2.5 \times 10^{-5} \exp(-2.1 \pm 0.3\ \mathrm{eV}/k_B T) \quad \left(\mathrm{cm^2\ s^{-1}}\right) \quad (4)$$

$$k = 5.4 \times 10^{-4} \exp(-1.2 \pm 0.03\ \mathrm{eV}/k_B T) \quad \left(\mathrm{cm\ s^{-1}}\right) \quad (5)$$

It must be noted that the activation energy for the oxygen surface exchange is lower than for the bulk diffusion, in agreement with reported data in other perovskite materials [23]. When comparing with the results on ionic conductivity, it is clear that the oxygen diffusion has an activation enthalpy much closer to the values observed by Belyakov [13].

Being in the nominally undoped region, it is difficult to explain the defect chemistry governing the concentration of oxygen vacancies. By comparing with other perovskites in the literature [14], it is clear that the oxygen transport in $SrZrO_3$ is by means of an oxygen vacancy mechanism. However, it is not clear which is the concentration of oxygen vacancies, since we do not know the type and concentration of possible impurities. For undoped material, normally only oxygen vacancies along with vacancies in the cation sublattice due to intrinsic disorder (Schottky) should exist, formed according to Eq. (6):

$$Sr_{Sr}^{x} + Zr_{Zr}^{x} + 3O_O^{x} \rightarrow V_{Sr}'' + V_{Zr}'''' + 3V_O^{\bullet\bullet} + SrZrO_3 \quad (6)$$

In this case, the observed activation energies for oxygen diffusion should be a sum of the activation enthalpy of formation of vacancies and of the activation enthalpy of migration.

In the case of extrinsic doping, the concentration of oxygen vacancies is fixed by the doping level. They can be formed by one of the reactions (Eq. (7) or (8)), depending if there is A- or B-site doping.

B-site doping with 3-valent cations, leads to creation of oxygen vacancies:

$$Me_2O_3 + 2Zr_{Zr}^{x} + 4O_O^{x} \rightarrow 2Me_{Zr}' + V_O^{\bullet\bullet} + 2ZrO_2 \quad (7)$$

A-site doping with 2-valent cations does not create oxygen vacancies:

$$MeO + Sr_{Sr}^{x} \rightarrow Me_{Sr}^{x} + SrO \quad (8)$$

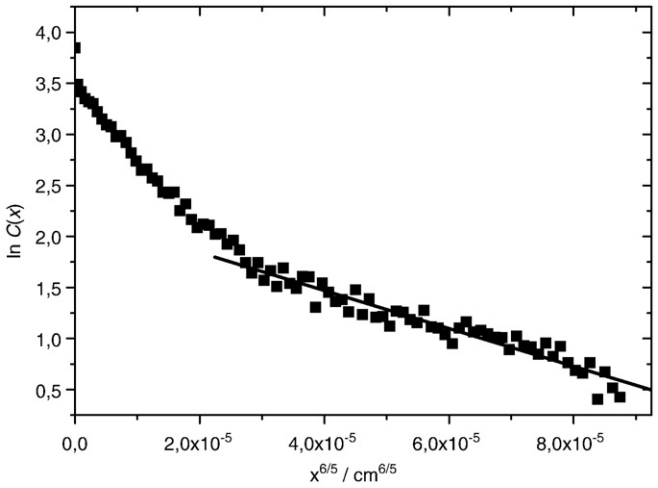

Fig. 5. $\ln C(x) = f(x^{6/5})$ for the sample heated at 1273 K.

Note that the presence of small amount of monoclinic zirconia in XRD may lead to practically B-site doped samples.

The observed activation energy of diffusion should then consist only of activation enthalpy of migration, and effects of doping may affect the pre-exponential factor. According to Haile et al. [17], the latter reaction should have a defect formation enthalpy of 0.7 eV. Since all Arrhenius graphs are pretty linear in the investigated temperature range, it is very likely that there is only one diffusion mechanism (in contrast, for example, to $BaCeO_3$ where a change of diffusion mechanism is reported [24]). However, as noted in the Introduction, the activation energies observed in nominally undoped $SrZrO_3$ are scattering significantly, suggesting that comparable, undoped $SrZrO_3$ are not easy to achieve. Combining the here observed activation energy of 2.1 eV with the activation enthalpy of conductivity measured by Belyakov [16], 2.2 eV, a difference of 0.1 eV remains. It should be noted that this value is much higher than typical values for oxygen diffusion in fluorites, but not unusual for perovskites.

Kilner et al. [23,25,26] largely developed correlations between oxygen diffusivity and surface exchange coefficient in a wide range of ABO_3 perovskite materials. They showed that if the activation enthalpy of surface reaction has half the activation enthalpy of bulk diffusion, then the oxygen vacancy concentration is mainly responsible of the isotopic surface exchange intensity. This also may hint to the conclusion that the samples investigated here are not undoped, but intrinsically doped.

3.2.2. Grain boundary diffusion

Le Claire proposed the following relation between the grain boundary diffusion coefficient and concentration at large sample depth [27]:

$$D_{gb}\delta = 0.661\left(\frac{4D_{vol}}{t}\right)^{1/2}\left[-\frac{\partial(\ln C(x))}{\partial x^{6/5}}\right]^{-5/3} \quad (9)$$

Here, D_{gb} is the grain boundary diffusion coefficient, δ the grain boundary width, D_{vol} the bulk diffusion coefficient, t the annealing time and $\frac{\partial(\ln C(x))}{\partial x^{6/5}}$ the slope of $\ln C(x) = f(x^{6/5})$ curve.

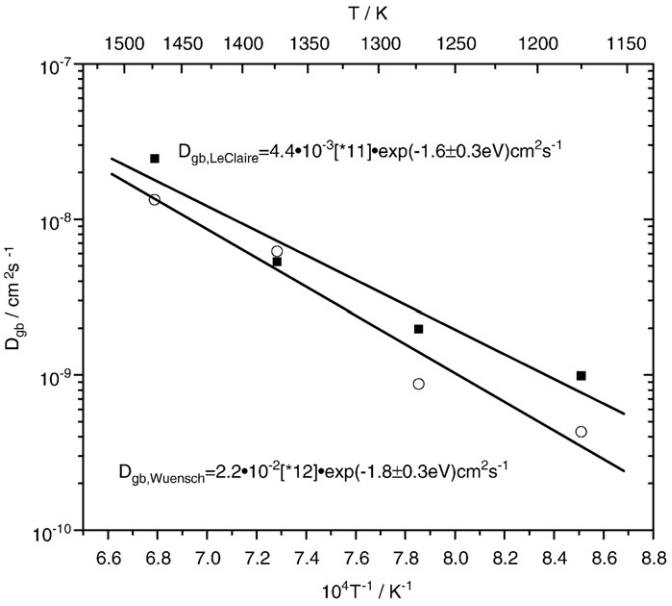

Fig. 6. Arrhenius plot of grain boundary diffusion coefficient evaluated according to the LeClaire equation (filled symbols) and to the Wuensch method (open symbols).

Fig. 5 represents $\ln C(x) = f(x^{6/5})$ obtained on a $SrZrO_3$ sample heated at 1273 K. The linear part at higher depth of this curve corresponds to grain boundary diffusion, and was taken to determine the slope $\frac{\partial(\ln C(x))}{\partial x^{6/5}}$ for calculating $D_{gb}\,\delta$ at each diffusion temperature. The resulting Arrhenius plot of the product $D_{gb}\,\delta$ is given in Fig. 6.

Assuming for δ the typical value of 1 nm [28], Eq. (10) holds for the grain boundary diffusion. An improved method for evaluating grain boundary diffusion profiles is given by Chung and Wuensch [29]. The results of a data analysis according to their method are also included in Fig. 6, Eq. (11), and in Table 1.

$$D_{gb,LeClaire} = 4.4\times10^{-3}\ \exp(-1.6\pm0.3\ \text{eV}/k_BT)\ \left(\text{cm}^2\ \text{s}^{-1}\right) \quad (10)$$

$$D_{gb,Wuensch} = 2.2\times10^{-2}\ \exp(-1.8\pm0.3\ \text{eV}/k_BT)\ \left(\text{cm}^2\ \text{s}^{-1}\right) \quad (11)$$

As can be seen, the difference between the two methods is small; however, the obtained activation enthalpy according to Wuensch is slightly higher than according to LeClaire (but the difference of 0.2 eV is within the experimental error of 0.3 eV for the two data sets). It has to be pointed out that the parameter β at high temperatures is smaller than the minimum value 10 given in reference [27], meaning that at this high temperature, the bulk diffusion is becoming to be so fast that the grain boundaries are no longer fully isolated.

Table 1 shows that the grain boundary diffusion coefficient of oxygen is three to four orders of magnitude higher than the bulk diffusion D_{vol}. These results indicate that at temperature treatments below 1373 K, grain boundaries are preferential diffusion pathways of oxygen in small-grained $SrZrO_3$ material. The activation enthalpy for grain boundary diffusion is lower than for bulk diffusion, about 75–85%, depending on the evaluation method in Eqs. (10) and (11). For metals, but also for

Table 1
Bulk diffusion coefficient D_{vol}, surface exchange coefficient k and grain boundary diffusion coefficient D_{gb} of oxygen in $SrZrO_3$ samples according to the LeClaire evaluation (index L) and the Wuensch Method (index W).

T (K)	D_{vol} (cm^2 s^{-1})	k (cm s^{-1})	$D_{gb,L}$ (cm^2 s^{-1})	β_L	$D_{gb,W}$ (cm^2 s^{-1})	β_W
1173	2.3×10^{-14}	3.6×10^{-9}	9.9×10^{-10}	85.6	4.3×10^{-10}	74.8
1273	1.2×10^{-13}	9.7×10^{-9}	2.0×10^{-9}	14.4	8.7×10^{-10}	12.8
1373	2.9×10^{-13}	2.0×10^{-8}	5.3×10^{-9}	10.2	6.2×10^{-9}	24.0
1473	1.9×10^{-12}	4.1×10^{-8}	2.5×10^{-8}	2.8	1.3×10^{-8}	3.1

Also included are the β-values (β_L) according to [27].

oxides [24], in general the activation enthalpy of grain boundary diffusion is 0.6 to 0.8 of the value of bulk diffusion [24], which is in agreement with the results obtained here.

4. Conclusion

In this study, dense $SrZrO_3$ polycrystalline materials were prepared in order to perform an oxygen tracer diffusion study. Oxygen isotopic exchange and SIMS characterization were used in order to determine surface exchange coefficients as well as bulk diffusion, and grain boundary diffusion coefficients of oxygen. Between 1173 K and 1473 K, oxygen diffusion is not limited by surface exchange and grain boundaries are fast pathways for oxygen diffusion. Activation energies for oxygen bulk diffusion are 2.1 eV, while for grain boundary diffusion 1.8 eV was observed. It is suggested that the samples might not be undoped, but contain some impurities acting as doping element.

Acknowledgements

We would like to thank F. Jomard, CNRS Meudon, France, for performing reference SIMS measurements and MAE-DAAD for funding through the PROCOPE program.

References

[1] P. Strunz, G. Schumacher, R. Vassen, A. Wiedenmann, V. Ryukhtin, Scr. Mater. 55 (2006) 545.
[2] H. Iwahara, T. Esaka, H. Uchida, N. Maeda, Solid State Ionics 3/4 (1981) 359.
[3] H. Iwahara, in: P. Colomban (Ed.), Proton Conductors, Cambridge University Press, Cambridge, UK, 1992, p. 511.
[4] H. Yugami, Y. Shibayama, T. Hattori, M. Ishigame, Solid State Ionics 79 (1995) 171.
[5] E. Matsushita, T. Sasaki, Solid State Ionics 125 (1999) 31.
[6] D. Hassan, S. Janes, R. Clasen, J. Eur. Ceram. Soc. 23 (2003) 221.
[7] W. Zheng, W. Pang, G. Meng, Solid State Ionics 108 (1998) 37.
[8] H.-Q. Ling, A.-D. Li, D. Wu, Y.-F. Tang, Z.-G. Liu, N.-B. Ming, Mater. Chem. Phys. 75 (2002) 170.
[9] C.-Y. Liu, C.-C. Chuang, J.-S. Chen, A. Wang, W.-Y. Jang, J.-C. Young, K.-Y. Chiu, T.-Y. Tseng, Thin Solid Films 494 (2006) 287.
[10] A. Meldrum, L.A. Boatner, W.J. Weber, R.C. Ewing, J. Nucl. Mater. 300 (2002) 242.
[11] H. Grübmeier, A. Naoumidis, G. Stochniol, A. Tsoga, Fresenius' J. Anal. Chem. 353 (1995) 393.
[12] J.A. Labrincha, F.M.B. Marques, J.R. Frade, J. Mater. Sci. 30 (1995) 2785.
[13] A.V. Belyakov, L.B. Borovkova, Yu.D. Novov, N.T. Dzhigailo, Translated from, Ogneupory 8 (1993) 11.
[14] J. Müller, K.-D. Kreuer, J. Maier, S. Matsuo, N. Ishigame, Solid State Ionics 97 (1997) 421.
[15] A. De Pretis, V. Longo, F. Ricciardiello, O. Sbraizero, Silic. Ind. 7–8 (1984) 139.
[16] E.A. Slonimskaya, A.V. Belyakov, Glass Ceram. 58 (2001) 54.
[17] S.M. Haile, G. Staneff, K.H. Ryu, J. Mater. Sci. 36 (2001) 1149.
[18] R.A. de Souza, G. Gibson, J.A. Kilner, Br. Ceram. Proc. 56 (1996) 95.
[19] R.A. De Souza, J.A. Kilner, C. Jeynes, Solid State Ionics 97 (1997) 409.
[20] E. Boehm, J.-M. Bassat, M.C. Steil, P. Dordor, F. Mauvy, J.-C. Grenier, Solid State Sci. 5 (2003) 973.
[21] J.D. Crank, Mathematics of Diffusion, Oxford University Press, Oxford, OX2 6DP, UK, 1975, p. 36.
[22] J. Philibert, Atom Movements, Diffusion and Mass Transport in Solids. Les Editions de Physique, France, 1991.
[23] J.A. Kilner, R.A. De Souza, I.C. Fullarton, Solid State Ionics 86–88 (1996) 703.
[24] M. Kilo, Defect Diffus. Forum 242–244 (2005) 185.
[25] S.J. Skinner, J.A. Kilner, Solid State Ionics 135 (2000) 709.
[26] R.A. De Souza, J.A. Kilner, J.F. Walker, Mater. Lett. 43 (2000) 43.
[27] A.D. Le Claire, Br. J. Appl. Phys. 14 (1963) 351.
[28] A. Atkinson, R.I. Taylor, Phil. Mag. A43 (1981) 979.
[29] Y.-C. Chung, B.L. Wuensch, J. Appl. Phys. 79 (1996) 8323.